Enzyme-Mimic Activity of Ferric Nano-Core Residing in Ferritin and Its Biosensing Applications

ARTICLE *in* ANALYTICAL CHEMISTRY · SEPTEMBER 2011

Impact Factor: 5.64 · DOI: 10.1021/ac202049q · Source: PubMed

5 AUTHORS, INCLUDING:

Hong-Xing Wu
Health Canada
219 PUBLICATIONS **16,019** CITATIONS
SEE PROFILE

Youyu Zhang
Hunan University
118 PUBLICATIONS **1,925** CITATIONS
SEE PROFILE

Zhaohui Li
Zhengzhou University
23 PUBLICATIONS **1,354** CITATIONS
SEE PROFILE

Yuehe Lin
Washington State University
364 PUBLICATIONS **21,422** CITATIONS
SEE PROFILE

Biomaterials 32 (2011) 1611–1618

Contents lists available at ScienceDirect

Biomaterials

journal homepage: www.elsevier.com/locate/biomaterials

Direct evidence for catalase and peroxidase activities of ferritin–platinum nanoparticles

Jia Fan [a,b], Jun-Jie Yin [c], Bo Ning [a], Xiaochun Wu [a], Ye Hu [d], Mauro Ferrari [d], Gregory J. Anderson [e], Jingyan Wei [b,*], Yuliang Zhao [f,*], Guangjun Nie [a,*]

[a] CAS Key Laboratory for Biological Effects of Nanomaterials & Nanosafety, National Centre for Nanoscience and Technology, 11 Beiyitiao, ZhongGuanCun, Beijing 100190, China
[b] College of Pharmaceutical Science, Jilin University, Changchun 130021, China
[c] Center for Food Safety and Applied Nutrition, Food and Drug Administration, College Park, MD 20740, USA
[d] Department of Nanomedicine and Biomedical Engineering, The University of Texas Health Science Center at Houston, Houston, TX 77031, USA
[e] Queensland Institute of Medical Research, Royal Brisbane Hospital, Queensland 4029, Australia
[f] CAS Key Laboratory for Biological Effects of Nanomaterials & Nanosafety, Institute of High Energy Physics, Chinese Academy of Sciences, China

ARTICLE INFO

Article history:
Received 16 September 2010
Accepted 3 November 2010
Available online 26 November 2010

Keywords:
Biomimetic enzymes
Catalase activities
ESR
Ferritin
Nanoparticles

ABSTRACT

Using apoferritin (apoFt) as a nucleation substrate, we have successfully synthesized 1–2 nm platinum nanoparticles (Pt–Ft) which are highly stable. By directly measuring the products of Pt–Ft-catalyzed reactions, we showed, with no doubt, Pt–Ft possesses both catalase and peroxidase activities. With hydrogen peroxide as substrate, we observed oxygen gas bubbles were generated from hydrogen peroxide decomposed by Pt–Ft; the generation of oxygen gas strongly supports Pt–Ft reacts as catalase, other than peroxidase. While with organic dyes and hydrogen peroxide as substrates, distinctive color products were formed catalyzed by Pt–Ft, which indicates a peroxidase-like activity. Interestingly, these biomimetic properties showed differential response to pH and temperature for different reaction substrates. Pt–Ft showed a significant increase in catalase activity with increasing pH and temperature. The HRP-like activity of Pt–Ft was optimal at physiological temperature and slightly acidic conditions. Our current study demonstrates that Pt–Ft possesses both catalase and peroxidase activities for different substrates under different conditions.

1. Introduction

Manufactured nanostructures that mimic enzymes are of great interest as they potentially have improved properties relative to native enzymes, such as greater resistance to extremes of pH and temperature and lower sensitivity to proteases. Many nanostructures that possess oxidase or peroxidase activities have been discovered [1–5]. Examples include peroxidase-like activity of ferromagnetic nanoparticles (NPs) [5] and oxidase mimetic properties of ceria oxide NPs [4]. These enzymatic activities look like the intrinsic properties for metals or metal oxides NPs and the antioxidative enzymatic activities of these NPs have shown great potential in prevention of oxidative stress associated cell death and disease progression in various experimental models [6,7]. Although the reaction substrates vary from hydrogen peroxide and superoxide anion to various peroxides and organic dyes, few of the previous studies provide direct evidence for the products generated. For example, hydrogen peroxide can generate either oxygen decomposed by catalase or water catalyzed by glutathione peroxidase [8]. It will be difficult to conclude what enzymatic properties a nanostructure possesses by measuring decreases in substrate concentration, as opposed to monitoring the generation of new products.

Ferritins are a well-studied family of proteins that play an important role in iron storage. They comprise 24 subunits that assemble into a hollow nanocage with an external diameter of 12 nm and an 8 nm diameter cavity [9]. Physiologically, iron is stored within the protein shell in a compact mineral form and one protein shell can accommodate up to 4500 atoms of iron. The

Abbreviations: apoFt, apoferritin; Pt–Ft, platinum nanoparticles; NPs, nanoparticles; Pt, platinum; ROS, reactive oxygen species; TMB, 3,3′,5,5′-tetramethylbenzidine; DAB, 3,3′-diaminobenzidine; CTPO, 3-carbamoyl-2,2,5,5-tetramethyl-3-pyrroline-1-yloxyl; DEPMPO, 5-diethoxyphosphoryl-5-methyl-1-pyroline-N-oxide; TEM, transmission electron microscopy; EDX, energy dispersive X-ray spectroscopies; HRP, horse radish peroxidase; ICP-OES, inductively coupled plasma optical emission spectrometry; BCA, bicinchoninic acid assay.

* Corresponding authors. Tel.: +86 10 82545529; fax: +86 10 62656765
E-mail addresses: jingyanwei@yahoo.com.cn (J. Wei), zhaoyuliang@ihep.ac.cn (Y. Zhao), niegj@nanoctr.cn (G. Nie).

0142-9612/$ – see front matter © 2010 Elsevier Ltd. All rights reserved.
doi:10.1016/j.biomaterials.2010.11.004

channels formed at the subunit junctions are required for the transport of iron and other metal ions into and out of the protein shell [9]. Ferritins have successfully been used as a scaffold to synthesize various protein-inorganic hybrids, such as FeS, CdS, CeSe and ZnSe [3,10–25]. For example, ferritin–gadolinium NPs have been used for magnetic resonance imaging (MRI) contrast agent [25], and ferritin–platinum for cytoprotection against free radicals [26].

Platinum (Pt) is one of the most widely used catalysts in chemical industries. Pt NPs recently have been demonstrated to scavenge both H_2O_2 and superoxide anion ($O_2^{\bullet-}$) [27,28]. These characteristics resemble the enzymatic activities of catalase and superoxide dismutase (SOD), two enzymes which play important roles in maintaining redox balance in living organisms by scavenging excess reactive oxygen species (ROS). The overproduction of ROS can lead to oxidative stress, damage to virtually all biomolecules and ultimately may induce cell death [29,30].

Compared to the numbers of studies in biomimetic syntheses of gold and silver, protein-guided formation of platinum, one of the most important noble metals, is relatively underexplored [31]. Especially, few previous studies have investigated the end-products of Pt NP catalyzed reactions. As part of a strategy aimed at generating bioactive, non-toxic and stable nanostructures with catalytic activities, in this study we have designed and synthesized Pt–Ft nanostructure, in which the apoferritin (apoFt) protein shell has been used as a nanoreactor to control the synthesis of size-tunable Pt nanostructures. We have investigated the enzymatic activities of Pt–Ft and the reaction mechanism catalyzed by Pt–Ft via directly measuring end product formation and the Pt valence states in the Pt–Ft.

2. Methods

2.1. Materials

ApoFt was obtained from Sigma–Aldrich at a concentration of 49 mg/mL in 0.15 M NaCl solution. Catalase (power) from bovine liver was obtained from Sigma–Aldrich. Horse radish peroxidase (power) was obtained from Beijing Biosynthesis Biotechnology Co. (Beijing). K_2PtCl_4, NaAc, H_2O_2, H_3BO_3, H_3PO_4 and citric acid were purchased from Beijing Chemical Works (Beijing). 3-carbamoyl-2,2,5,5-tetramethyl-3-pyrroline-1-yloxyl (CTPO) and catalase (from bovine liver) were purchased from Sigma chemical Co. (St. Louis, MO). 5-Diethoxyphosphoryl-5-methyl-1-pyroline-N-oxide (DEPMPO) was from Radical Vision (Marseille, France).

2.2. Preparation of Pt–Ft

An apoFt solution (1 μM, 2.5 mL) was mixed with K_2PtCl_4 (24 mM, 126 μL) and the reaction solution was adjusted the solution to pH 8.5 using 0.2 M NaOH, followed by stirring for 2 h at room temperature. Then a solution of $NaBH_4$ (0.2 M, 150 μL) was added to the mixture and stirred for 3 h at room temperature. To avoid any by-product, Pt–Ft composite was purified by size-exclusion chromatography (Sephacryl S-300), using deionized water as elution buffer, and the first peak was collected at 280 nm monitored by Ultraviolet Detector.

2.3. Mimetic peroxidase activity assays

The catalase-like activity assays were carried out at 37 °C using catalase assay kit (Beyotime Institute of Biotechnology, Shanghai) according to the manufacturer's instructions. Pt–Ft (20 μg, containing 250 ng Pt) or 8.3 ng catalase were added to 30 μL Teorell-Stenhagen buffer (T-S buffer, 33 mM citric acid, 33 mM phosphoric acid, 23 mM boric acid, pH = 7.4) in the presence of 83 mM H_2O_2. After 5 min reaction, the solution was diluted 50 times by T-S buffer, and then the residual H_2O_2 was monitored at 520 nm using Tecan infinite 200 spectrophotometer.

Catalase-like activity of Pt–Ft was also evaluated in the H_2O_2/UV system, which generates hydroxyl radicals. Under UV irradiation hydrogen peroxide produces hydroxyl radicals which were detected using the spin trap DEPMPO. The effect of Pt–Ft on this system was studied and compared to that of catalase. Reaction mixtures contained 14 mM DEPMPO, 5 mM H_2O_2, and different concentrations of catalase or Pt–Ft. Samples were placed in quartz capillary tubes and exposed to UV light (270 nm). ESR spectra of the DEPMPO/OH adducts were measured every 5 min for 20 min. After the experiments were done, gas bubbles were observed in the capillary tubes for both catalase and Pt–Ft samples. ESR spin label oximetry was used to further investigate oxygen generation. A stock solution containing CTPO, a water soluble spin label, and H_2O_2 was deoxygenated with N_2. Different concentrations of catalase or Pt–Ft were then added and samples transferred into 50 μL glass capillary tubes, sealed, and placed in the ESR cavity. Final concentrations were 0.1 mM CTPO and 0.25 mM H_2O_2 in 50 mM PBS (pH 7.4, chelex treated). ESR experiments were run on a Bruker EMX spectrometer. For spin trapping experiment, ESR signals were obtained with 20 mW incident microwave power, 1 G field modulation, sweep width 20 G, and time constant of 163.84 ms. A light system consisting of a Xenon lamp coupled with a Schoeffel monochromator was used to generate UV light at 270 nm for the H_2O_2/UV experiments. For ESR oximetry, instrument setting was 1 mW microwave power, 0.04 G field modulation, and 5 G sweep width.

HRP-like activity was measured with 15 μg Pt–Ft (containing 187.5 ng Pt) or 1.25 ng HRP in 100 μL sodium acetate buffer (pH = 4), in the presence of 210 μM TMB and 8 mM H_2O_2 at 37 °C. After 5 min, the color formation was monitored at 450 nm using Tecan infinite 200 spectrophotometer after adding 2 M H_2SO_4 to stop the reaction.

The apparent kinetic parameters were calculated based on Michaelis equation [32].

$v = Vmax \times [S]/(Km+[S])$, v is the initial velocity, $Vmax$ is the maximal reaction velocity, [S] is the concentration of substrate and Km is the Michaelis constant. Km and $Vmax$ were obtained by Lineweaver–Burk plot method.

2.4. Transmission electron microscopy

A 5 μL solution of Pt–Ft or Pt nanoparticles was dropped onto amorphous-carbon-coated copper grids. For negative staining, 10 μL of uranyl acetate solution was dropped onto the grids for 10 min and the excess solution was removed with a filter paper. The TEM images were obtained using a Tecnai G2 F20 U-TWIN transmission electron microscope.

2.5. Measurement of the amount of platinum in ferritin

Pt–Ft was dissolved in the fresh mixture of concentrated nitric acid and hydrochloric acid (volumetric ratio of 1:3) to form chloroplatinic acid and then the Pt content was determined by ICP-OES. ApoFt was quantified by the bicinchoninic acid (BCA) method.

3. Results and discussion

3.1. Preparation and characterization of Pt–Ft

To prepare Pt–Ft, a solution of apoFt was treated with 100–1000 M equivalents of K_2PtCl_4 to form a homogenous orange solution. To increase the electrostatic interaction between Pt ions and interior surface of apoFt, the solution was adjusted to pH 8.5. The solution was stirred for 2 h at room temperature. Pt ions were reduced by adding $NaBH_4$ to yield zero-valent Pt NPs (Scheme 1). After 3 h, the color of the solution changed to dark brown, with the intensity varying depending on the amount of Pt ions used. The absorption spectra also changed during reduction. The initial protein solution showed one peak at 280 nm; two small absorption peaks appeared at 305 and 380 nm after mixing with Pt ions. Finally the two small peaks are replaced with a broad absorption spectrum, which is typical for Pt colloids after reduction reactions (Fig. S1a). A similar change in absorption spectrum has been observed for Pt particles coated with polymers or dendrimers synthesized in organic solvents (such as, ethyl alcohol) at high temperature (100–200 °C) [27]. In contrast, for Pt–Ft synthesis, we were able to use much milder conditions (room temperature and

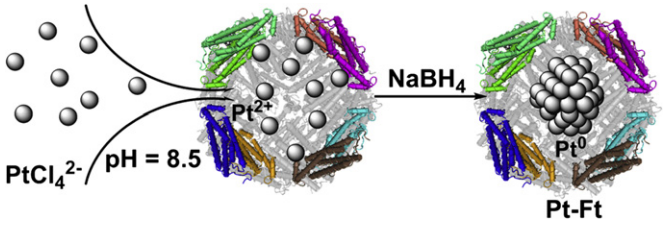

Scheme 1. Schematic illustration of the synthesis route of Pt–Ft.

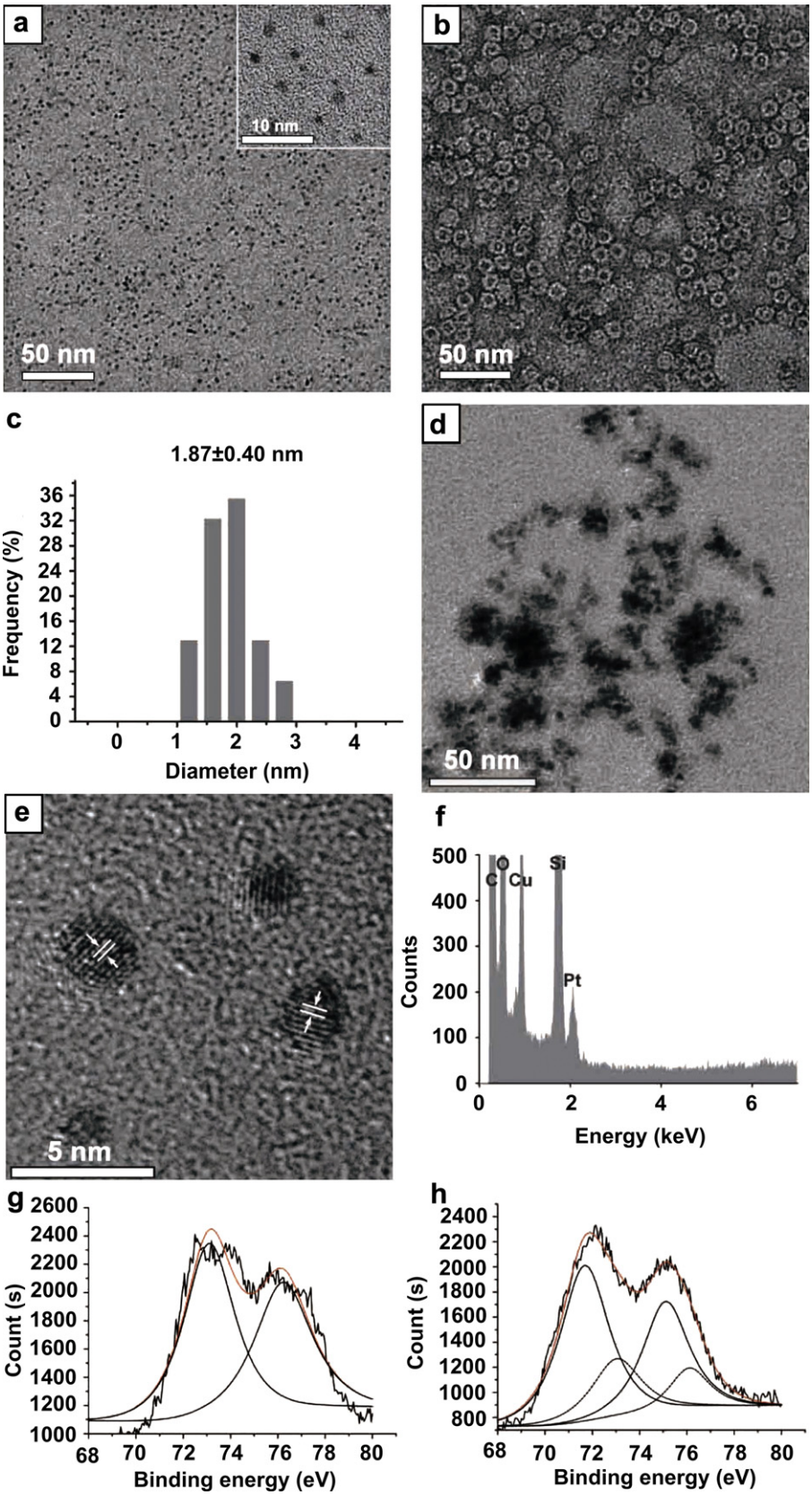

Fig. 1. Characterization of Pt–Ft by TEM (a–e), EDX (f) and XPS (g–h). a) An unstained sample and a magnified image (inset); b) A sample negatively stained with uranyl acetate; c) Histogram of the size of Pt nanoclusters. d) Pt reduced by $NaBH_4$ without apoFt; e) High-resolution TEM image of unstained Pt–Ft; f) EDX spectrum of Pt–Ft showing the Pt peak. XPS spectra in the Pt(4f) region of apoFt and K_2PtCl_4 complexes before reduction (g) and after reduction by Pt–Ft $NaBH_4$ (h).

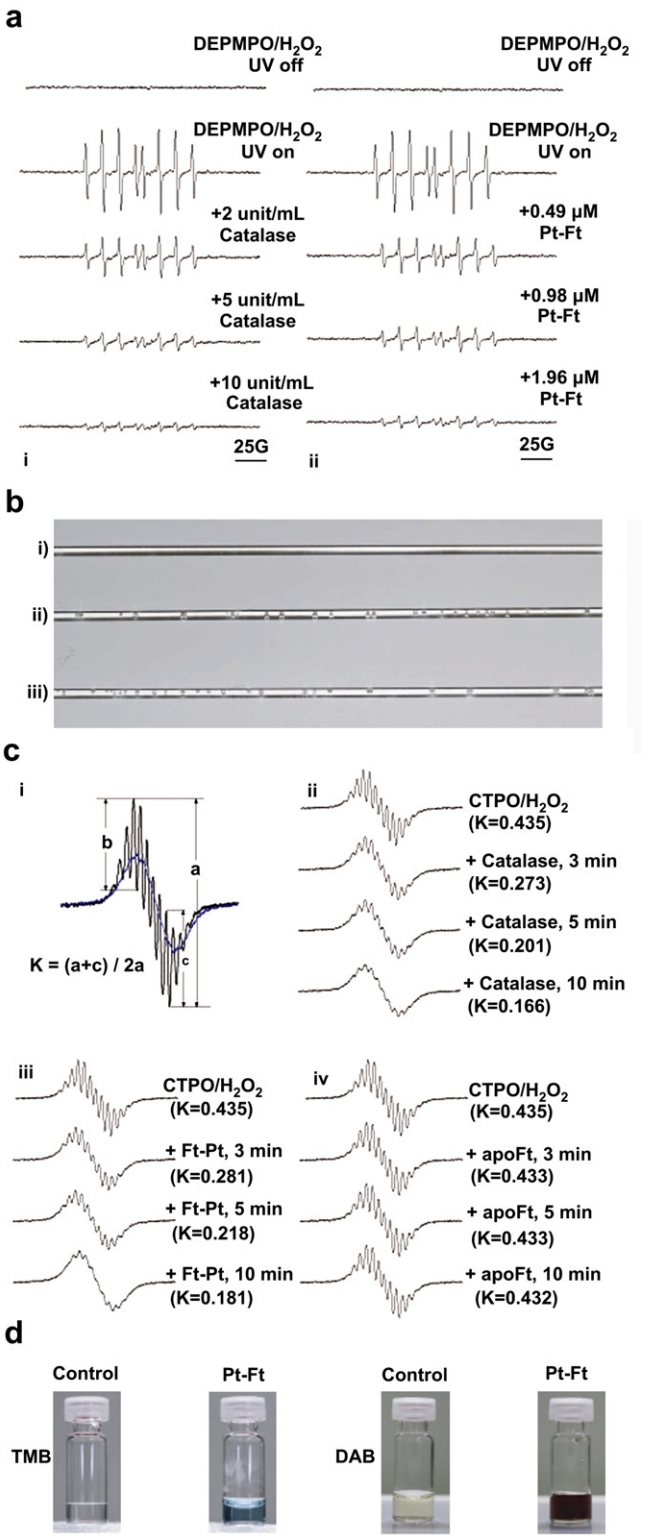

Fig. 2. Direct measurement of the end-products of Pt–Ft catalyzed reactions. (a) The effects of catalase (ai) and Pt–Ft (aii) on hydroxyl radical formation in H_2O_2/UV system. ESR signal was recorded after 20 min of UV irradiation; (b) After the UV/H_2O_2 with catalase/Pt–Ft experiment, gas bubbles were observed in the quartz capillary tubes. Sample containing 14 mm DEPMPO/5 mM H_2O_2 alone (bi); mixed with 10 u/mL catalase (bii); and 1.96 μM Pt–Ft (biii); (c) Quantitative measurement of oxygen gas production. Illustrates the super hyperfine structure of the center field line from ESR spectra of CTPO in nitrogen-saturated (black) and air-saturated (blue) solution of 0.1 mM CTPO mixed with 0.25 mM H_2O_2 in PBS buffer (pH 7.4). The K parameter is used to determine oxygen concentration, and is calculated by the equation K = (b + c)/2a, where a, b and c are determined as shown in (ci). Oxygen generation was measured in a closed chamber with samples containing 95 μM CTPO, 247 μM H_2O_2 mixed with (cii) 1 unit/mL catalase; (ciii) 0.245 μM Pt–Ft; and (civ) 0.245 μM ApoFt in PBS buffer. The numbers in brackets represent the calculated K parameter (the value of the K parameter is inversely proportional to the oxygen concentration). All spectra were recorded at room temperature; microwave power 1 mW, modulation amplitude 0.05 G, and scan range 5 G. (d) Pt–Ft catalyzed the formation of colored oxidation products of TMB (blue) and DAB (brown).

aqueous solution). To avoid any by-product, Pt–Ft was purified by size-exclusion chromatograph (Sephacryl S-300).

Transmission electron microscopy (TEM) images showed that the Pt NPs were largely monodispersed and roughly spherical (Fig. 1a). After negative staining with uranyl acetate, Pt nanoclusters were observed within the ferritin shell by TEM (Fig. 1b). Over 90% of the ferritin nanocages contained visible Pt NPs (over 100 protein core-shell structures counted in Fig. 1b). The Pt NPs have an average diameter of 1.87 ± 0.40 nm as shown in the histogram (Fig. 1c). In the absence of apoFt, a black amorphous precipitate was observed (Fig. 1d). In contrast, the Pt–Ft preparation remained a clear, dark brown solution for weeks at room temperature. High-resolution TEM images indicated a continuous lattice spacing of 0.224 nm (Fig. 1e), which corresponds to the (111) facet of an fcc Pt crystal. Energy dispersive X-ray spectroscopies (EDX) confirmed that it was Pt, but not iron in the protein cage (Fig. 1f). These results suggest the specific formation of Pt NPs inside the apoFt nanocage. The platinum 4f electron spectra are shown in Fig. 1g (before reduction) and 1 h (after reduction) by X-ray photoelectron spectroscopy (XPS). Fig. 1g showed that before reduction, the Pt $4f_{7/2}$ lies at 73.0 eV, which is close to the reported binding energy of K_2PtCl_4. The Pt 4f electron spectra of Pt–Ft was well-resolved with two doublets with Pt $4f_{7/2}$ binding energies of 71.7 and 73.0 eV (Fig. 1h). The line at lower binding energies is due to Pt^0 [33], while the higher binding energy component is due to a Pt^{2+} species such as PtO [34]. The XPS spectra also indicated that Pt–Ft NPs were composed of 74% of Pt^0 and 26% of Pt^{2+}. Dynamic light scattering (DLS) experiments provided measurement for the average hydrodynamic diameters of apoFt and Pt–Ft (15.91 and 15.22 nm, respectively, Fig. S1b and c in the supporting information). Zeta potential is an index of the magnitude of the interaction among particles and commonly used to assess the stability of NPs. ApoFt exhibits a negative potential of −27 mV. Under the same conditions, Pt–Ft shows the same potential of −27 mV. Therefore, the integrality and stability of apoFt has not been affected by the in situ synthesis of Pt NPs.

3.2. Measuring end product formation

To examine whether Pt–Ft could facilitate the decomposition of hydrogen peroxide as observed in catalase, we investigated this enzymatic activity in several systems. First, we chose H_2O_2/UV DEPMPO spin trap system to evaluate the effects of Pt–Ft on hydroxyl radical signal intensity. This system was previously used to detect hydroxyl radical formation [35]. Pt–Ft was observed to reduce the DEPMPO/$OH^{\cdot}$ adduct signal intensity in a dose and time dependent fashion. Even the low dose of Pt–Ft (0.49 μM) resulted in a significant reduction in signal intensity (Fig. 2a). Similar results were obtained when catalase was tested on the same system, suggesting possible similarity in catalytic activity. In addition, gas bubbles were observed in the capillary tubes with samples containing catalase or Pt–Ft (Fig. 2b). More bubbles continued to form long after the experiment was over and the UV light turned off. This observation shows that the generation of the bubbles was not a result of UV light irradiation. Also, in the closed system, the bubbles could only have been generated within the system.

Catalase is known to decompose hydrogen peroxide to form water and molecular oxygen, thus implying that the observed gas bubbles was oxygen, at least in the case of catalase.

Similarly to catalase, the active site of native horse radish peroxidase (HRP) composes of heme prosthetic group. This allows us to investigate whether Pt–Ft could facilitate the oxidation of a series of organic dyes as the substrates of HRP. We chose TMB and DAB, which were commonly used as the substrates of HRP in various enzymatic assays. As shown in Fig. 2d, Pt–Ft catalyzed both TMB and DAB oxidation in the presence of hydrogen peroxide, as demonstrated by the appearance of the characteristic color of oxidized TMB (blue) or DAB (brown). In the absence of Pt–Ft, auto-oxidation of DAB and TMB was negligible.

3.3. Catalase and peroxidase activities of Pt–Ft

Furthermore, the catalase-like activity of Pt–Ft was monitored at different pHs and temperatures by measuring the absorption of residual hydrogen peroxide at 520 nm. Interestingly, while catalase had a pH optimum of 8–9 and temperature optimum of 37 °C, the catabolism of H_2O_2 by Pt–Ft continued to increase up to pH 12 (Fig. 3a). Furthermore, the catalytic activity increased as the reaction temperature was raised and was greatest at the highest temperature studied (85 °C) (Fig. 3b). By increasing both pH and temperature (60 °C, pH 12), a synergetic effect was observed. The measured catalytic activity was higher than that observed when pH or temperature was increased separately (Fig. S2 in supporting information). The stability of H_2O_2 itself at different pH or different temperature was measured. The results showed that H_2O_2 did not self-decompose under all experiment conditions (Fig. S3 in supporting information). It is generally accepted that surface Pt atoms are oxidized in electrochemical processes, and that hydrogen ions are released simultaneously [36]. This is a reversible process. We infer that in an alkaline solution, the hydroxyl ion would facilitate the formation of platinum oxide. This may explain, at least partially, the increases in catalase-like activity observed under basic conditions. As the temperature increases, the rate of molecular motion speeds up, increasing interaction between Pt NPs and hydrogen peroxide. Thus, Pt NPs showed higher catalase-like activity at higher temperature.

For the catalase-like activity, Michaelis–Menten-like curves were obtained under low concentrations of hydrogen peroxide for Pt–Ft (<2 M) and for the native catalase (<500 mM) (Table 1 and Fig. S4 in supporting information, which used to calculate the enzymatic parameters). It has been shown that catalases do not exhibit Michaelis–Menten kinetics over the complete substrate concentration range, but they do follow a Michaelis–Menten-like dependence of velocity on low concentrations of hydrogen

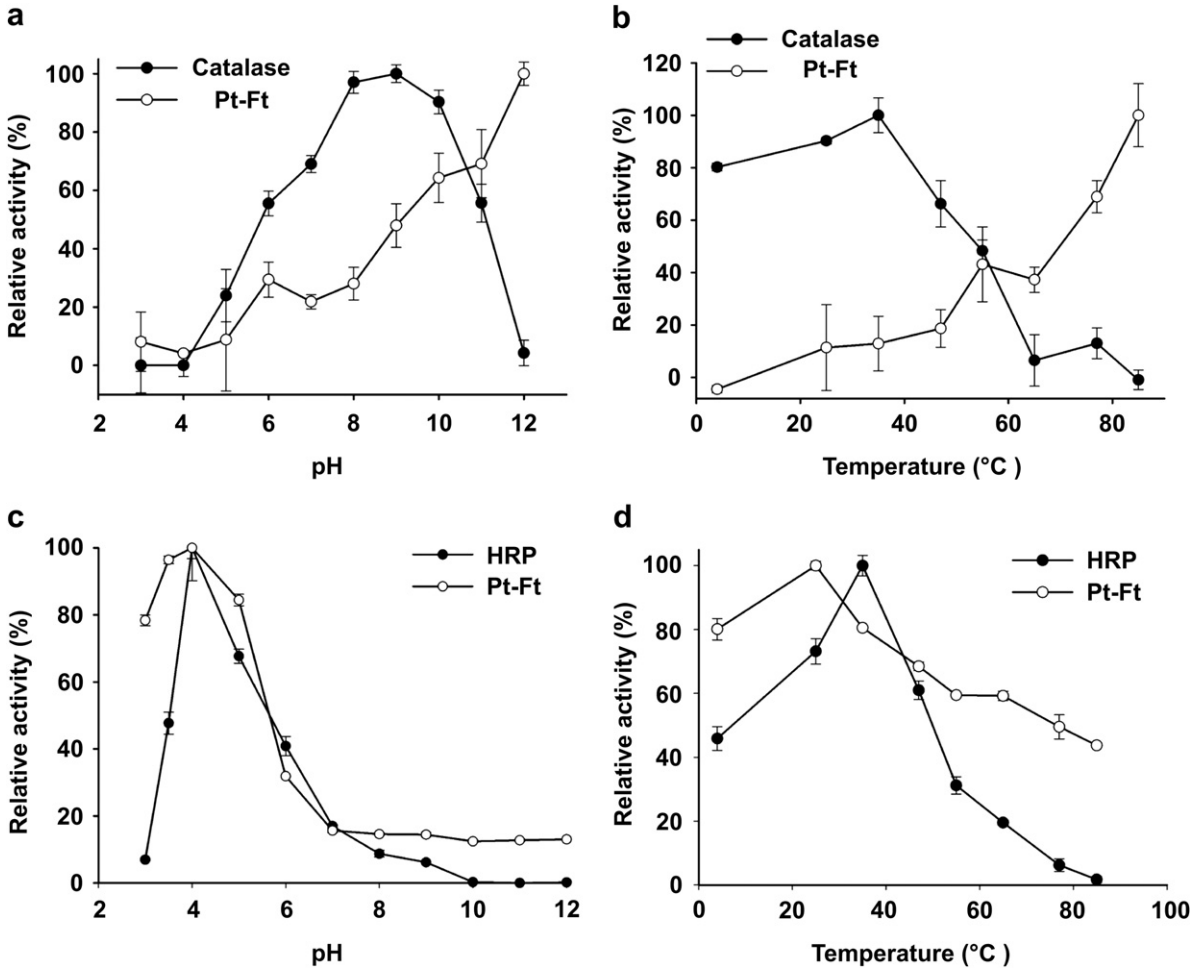

Fig. 3. The catalase-like activity of Pt–Ft is pH and temperature dependent (a and b). a) Catalase shows a pH optimum of 8–9, and the activity of Pt–Ft gradually increases as the pH increases; b) Catalase shows a temperature optimum of around 25–35 °C, and the activity of Pt–Ft gradually increases as the temperature increases. HRP-like activity of Pt–Ft is pH and temperature dependent (c and d); c) The optimal pH values of HRP and Pt–Ft were both at pH 4; d) The optimal temperatures of HRP and Pt–Ft were 37 and 25 °C, respectively. The maximum activity of enzymes in each curve was set as 100%.

Table 1
Comparison of the kinetic parameters of Pt–Ft and native enzymes.

	Substrate	*Km* (mM)	*Vmax* (mMs-1)
Catalase	H_2O_2	71.60	0.29
Pt–Ft[a]	H_2O_2	420.60	0.84
HRP	TMB	2.89	6.05×10^{-3}
Pt–Ft	TMB	0.22	5.58×10^{-4}
HRP	H_2O_2	4.37	4.78×10^{-3}
Pt–Ft[b]	H_2O_2	187.25	0.32

[a] The apparent *Km* value of catalase-like activity of Pt–Ft with H_2O_2 as a substrate.
[b] The apparent *Km* value of HRP-like activity of Pt–Ft with H_2O_2 as a substrate.

peroxide [37]. The apparent *Km* of Pt–Ft with hydrogen peroxide as the substrate was about 6 times higher than catalase (Table 1), suggesting a significant lower affinity for hydrogen peroxide compared to catalase. At higher concentrations of hydrogen peroxide (above 1 M), inactivation of catalytic activities was apparent for the native catalase, but not significant for Pt–Ft (data not shown). The resistance to high concentration of substrate is another important feature for Pt–Ft as a biomimetic catalase.

Next, we examined the HRP-like activities of Pt–Ft at different pHs and temperatures. For these studies, H_2SO_4 was added to stabilize the TMB oxidation product and the resulting yellow solution was monitored at 450 nm by UV–Vis spectrometry. Pt–Ft facilitated the oxidation of TMB at all pHs tested (from pH 3 to 12), with a pH optimum of around 4 (Fig. 3c), similar to that of native HRP. However, the optimal temperature of 25 °C was considerably lower than that of native HRP (37 °C) (Fig. 3d). Nevertheless, Pt–Ft retained HRP-like activity over a wide range of temperatures (from 4 to 85 °C) and overall maintained a greater percentage of activity than native HRP. Together, Pt–Ft possesses both catalase and peroxidase activities for different substrates.

Compared to other engineered metal oxide NPs, such as iron oxide and cerium oxide, Pt–Ft had a significantly smaller nanostructural core and unique peroxidase activities for different substrates [3,5]. Metal oxide NPs transfer electron between pairs of different oxidation states of metal ions, such as Fe^{2+}/Fe^{3+} and Ce^{3+}/Ce^{4+} to drive their catalytic activity [3,5]. However, we showed that Pt–Ft consists of mainly zero-valent Pt nanoclusters (Fig. 1f and g). The changes of valence states are between zero valence and oxidized Pt.

3.4. Comparison of stability of Pt–Ft and native enzymes

We further determined steady-state kinetic parameters for the oxidation of TMB by Pt–Ft in the presence of hydrogen peroxide.

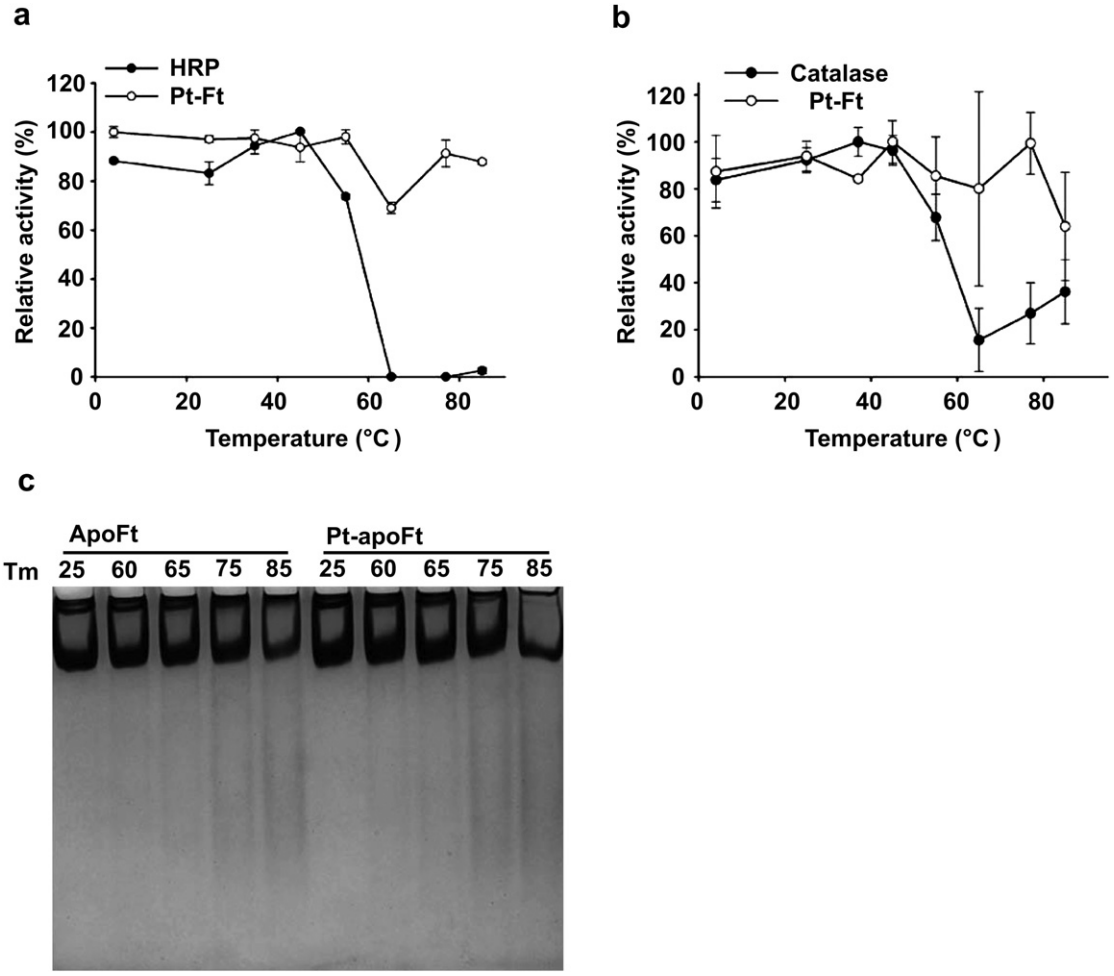

Fig. 4. Stability of Pt–Ft and native enzymes. a) Comparison of the stability of native HRP and HRP-like activity of Pt–Ft following different temperature pre-treatments; b) Comparison of the stability of native catalase and catalase-like activity of Pt–Ft following different temperature. Pt–Ft and the native enzymes were pre-incubated at temperatures from 4 to 85 °C for 2 h and then the activity was measured according to the procedure described in the method. The maximum activity of enzymes in each curve was set as 100%; c) Native-PAGE of apoFt and Pt–Ft after heat treatment. The samples were incubated at different temperatures (25, 60, 65, 75 or 85 °C respectively) prior to electrophoresis. The native gel (6%) was stained with Coomassie brilliant blue.

Typical Michaelis–Menten curves were obtained for Pt–Ft and HRP (Table 1 and Fig. S5 in supporting information, which used to calculate the enzymatic parameters). The apparent *Km* value of Pt–Ft with H_2O_2 as a substrate was significantly higher than that of HRP. It is similar to that of H_2O_2 oxidation by iron oxide NPs [5]. When TMB was used as a substrate, the apparent *Km* of Pt–Ft was 0.22 mM, about 13 fold lower than that of native HRP (Table 1), suggesting that Pt–Ft has a significantly higher affinity for TMB than the native enzyme. These results also suggest that the affinity of Pt–Ft for TMB was higher than that of iron oxide NPs, which have been reported to have an affinity 4 times higher than that of HRP [5]. The higher affinity of Pt–Ft likely reflects the large catalytic surface area of the small, homodisperse Pt NPs.

To examine the relative stabilities of Pt–Ft and native HRP, each preparation was pre-treated at different temperatures (4–85 °C) for 2 h prior to analyzing their ability to catalyze the oxidation of TMB. Pt–Ft showed similar activity over the temperature range studied, with only a slight decrease above 65 °C (Fig. 4a). Native HRP, however, lost most of its activity above 50 °C. Similar results were seen after pre-treatment at different pHs (3–12) (Fig. S6 in supporting information). Pt–Ft was stable over all pHs tested, while native HRP showed significant enzymatic activity only after pH 10 pre-treatment (around its optimal pH range). Taken together, these results demonstrate that Pt–Ft is capable of catalyzing the oxidation of organic dyes under various temperature and pH conditions. Although there were some similarities in the responses of Pt–Ft and native HRP to various environmental conditions, the former was more stable at high temperatures and extreme pHs.

We also compared the stability of the catalase-like activity of Pt–Ft to that of native catalase at various temperatures (Fig. 4b). Pt–Ft retained the ability to oxidize H_2O_2 at all temperature studied after 2 h pre-treatment, while native catalase lost the majority of its activity above 60 °C. Thus both the peroxidase and catalase-like activities of Pt–Ft are highly stable.

3.5. Determination of the amount of platinum in ferritin shell

Next, we assessed the effects of protein shell stability on the enzymatic activities of Pt–Ft. Both apoFt and Pt–Ft were incubated at various temperatures for 2 h, followed by electrophoresis under non-denaturing conditions. As shown in Fig. 4c, both apoFt and Pt–Ft were stable at or below 60 °C. When the temperature was over 65 °C, there was a slight reduction in the intensity of ferritin nanocage staining which may represent either dissociated ferritin subunits or degradation products. Significant loss of ferritin nanocage structures was only observed at 85 °C. These observations clearly demonstrated that even under high temperatures (up to 75 °C), there was little dissociation or degradation of the ferritin shell.

Since the biomimetic activities of Pt–Ft have been associated with the Pt core in the ferritin shell, controllable synthesis of Pt–Ft has been achieved by altering the ratios of Pt to apoFt. To measure Pt atom numbers in ferritin shell, the Pt levels were measured by inductively coupled plasma optical emission spectrometry (ICP-OES) while protein levels were measured using the bicinchoninic acid assay (BCA). As shown in Table 2, as the Pt to apoFt ratio was increased, the amount of Pt in Pt–Ft rose from 3 to 30 atoms per molecule. Further increases in the Pt ion concentration led to the formation of a precipitate that could be observed in TEM images (data not shown), suggesting the formation of large Pt particles outside the protein shell. As the number of Pt atoms in Pt–Ft increased, the peroxidase activity of the complex increased proportionally. Previous work has shown that ferritin catalyzes aromatic amine oxidation, such as the oxidation of TMB, resulting in the interaction of Fe^{3+} ions with H_2O_2 [38]. Therefore, we chose apoFt alone, which is a protein shell of ferritin lacking iron as a control. The result was shown in Table 2, that apoFt alone did not have any peroxidase activity. The highest enzymatic activity was observed when Pt–Ft was prepared with a molar ratio of Pt to apoFt of 1000:1. Since histidine residues have been shown to bind Pt ion with high affinity [31], it is possible that histidine residues in the apoFt protein shell are important for Pt ion binding. The limited number of potential binding sites in ferritin (six histidine residues in each Ft light chain) may be one of the factors limiting the core size of Pt–Ft. The numbers of Pt atoms per protein encapsulated is slightly lower than the calculation based on TEM images (Fig. 1). This slight difference may be due to the small size of the Pt NPs as they approach the boundaries of accurate measurement by TEM.

Table 2
Quantitative analyses of Pt atoms and HRP-like activity of Pt–Ft.

([Pt^{2+}]/[ApoFt]) in the reaction solution	Pt atoms/ferritin molecule	Relative activity of Pt–Ft (%)[a]
0:1	0	0
250:1	3.1 ± 0.1	2.2
500:1	7.2 ± 0.3	18.5
1000:1	30.0 ± 0.1	100
2000:1	precipitation[b]	NA

[a] The enzymatic activity of 1000:1 of Pt-apoFt as 100%.
[b] Precipitation appeared and formation of Pt particles outside of the protein shell.

4. Conclusion

In this study we investigated the possibility of using apoFt protein shell as a nanoreactor to control the synthesis of size-tunable Pt nanostructures. ApoFt was used as a scaffold to synthesize 1–2 nm Pt–Ft inside its protein shell. More importantly, we definitively showed that Pt–Ft possesses both catalase and peroxidase activities by directly measuring end product formation. With hydrogen peroxide as the substrate, we observed generation of oxygen gas bubbles as the hydrogen peroxide was decomposed by Pt–Ft; when organic dyes and hydrogen peroxide were used as substrates, distinctive colored products were formed catalyzed by Pt–Ft. Furthermore, Pt–Ft exhibited these enzymatic activities with distinctive enzymatic properties, namely different responses to pH and temperature for different enzymatic substrates. Using TMB and DAB as substrates, the optimal pH and temperature for the oxidation catalyzed by Pt–Ft were similar to that of native HRP (pH optimum 4; temperature optimum 37 °C). However, the optimal pH and temperature were quite different from that of native catalase, being significantly higher in each case. To the best of our knowledge, these enzymatic features have not been commonly seen in the native enzyme or in other nanostructures. The current study showed that Pt–Ft could be used as a non-toxic bio-catalyst in various biomedical situations, such as in various human diseases involved in oxidative stress damage.

Acknowledgements

This work was supported by grants from MOST 863 (2009AA03Z335), MOST 973 program (2010CB933600, 2011CB933403) and NSFC (10979011; 30900278). GN acknowledges the support of CAS Hundred Talents Program. We thank Herman Lutterodt for help with ESR study and Professor Sarah Perrett for her suggestions.

Appendix

Figure with essential color discrimination. Figs. 1 and 2, Scheme 1 in this article is difficult to interpret in black and white. The full color images can be found in the online version, at doi:10.1016/j.biomaterials.2010.10.004.

Appendix. Supplementary data

Supplementary data related to this article can be found online at doi:10.1016/j.biomaterials.2010.10.004.

References

[1] Dai ZH, Liu SH, Bao JC, Jui HX. Nanostructured FeS as a mimic peroxidase for biocatalysis and biosensing. Chem Eur J 2009;15:4321–6.
[2] Asati A, Santra S, Kaittanis C, Nath S, Perez JM. Oxidase-like activity of polymer-coated cerium oxide nanoparticles. Angew Chem Int Ed 2009;48:2308–12.
[3] Perez JM, Asati A, Nath S, Kaittanis C. Synthesis of biocompatible dextran-coated nanoceria with pH-dependent antioxidant properties. Small 2008;4:552–6.
[4] Korsvik C, Patil S, Seal S, Self WT. Superoxide dismutase mimetic properties exhibited by vacancy engineered ceria nanoparticles. Chem Commun; 2007:1056–8.
[5] Gao LZ, Zhuang J, Nie L, Zhang JB, Zhang Y, Gu N, et al. Intrinsic peroxidase-like activity of ferromagnetic nanoparticles. Nat Nanotechnol 2007;2:577–83.
[6] Chen J, Patil S, Seal S, McGinnis JF. Rare earth nanoparticles prevent retinal degeneration induced by intracellular peroxides. Nat Nanotechnol 2006;1:142–50.
[7] Schubert D, Dargusch R, Raitano J, Chan SW. Cerium and yttrium oxide nanoparticles are neuroprotective. Biochem Biophys Res Commun 2006;342:86–91.
[8] Day BJ. Catalase and glutathione peroxidase mimics. Biochem Pharmacol 2009;77:285–96.
[9] Harrison PM, Arosio P. Ferritins: molecular properties, iron storage function and cellular regulation. Biochim Biophys Acta 1996;1275:161–203.
[10] Ueno T, Suzuki M, Goto T, Matsumoto T, Nagayama K, Watanabe Y. Size-selective olefin hydrogenation by a Pd nanocluster provided in an apo-ferritin cage. Angew Chem Int Ed 2004;43:2527–30.
[11] Xing RM, Wang XY, Zhang CL, Zhang YM, Wang Q, Yang Z, et al. Characterization and cellular uptake of platinum anticancer drugs encapsulated in apoferritin. J Inorg Biochem 2009;103:1039–44.
[12] Xing RM, Wang XY, Yan LL, Zhang CL, Yang Z, Wang XH, et al. Fabrication of water soluble and biocompatible CdSe nanoparticles in apoferritin with the aid of EDTA. Dalton Trans; 2009:1710–3.
[13] Ueno T, Abe M, Hirata K, Abe S, Suzuki M, Shimizu N, et al. Process of accumulation of metal ions on the interior surface of apo-ferritin: crystal structures of a series of apo-ferritins containing variable quantities of Pd(II) ions. J Am Chem Soc 2009;131:5094–100.
[14] Turyanska L, Bradshaw TD, Sharpe J, Li M, Mann S, Thomas NR, et al. The biocompatibility of apoferritin-encapsulated PbS quantum dots. Small 2009;5:1738–41.
[15] Deng QY, Yang B, Wang JF, Whiteley CG, Wang XN. Biological synthesis of platinum nanoparticles with apoferritin. Biotechnol Lett 2009;31:1505–9.
[16] Yang Z, Wang XY, Diao HJ, Zhang JF, Li HY, Sun HZ, et al. Encapsulation of platinum anticancer drugs by apoferritin. Chem Commun; 2007:3453–5.
[17] Uchida M, Klem MT, Allen M, Suci P, Flenniken M, Gillitzer E, et al. Biological containers: protein cages as multifunctional nanoplatforms. Adv Mater 2007;19:1025–42.
[18] Li M, Viravaidya C, Mann S. Polymer-mediated synthesis of ferritin-encapsulated inorganic nanoparticles. Small 2007;3:1477–81.
[19] Knez M, Kadri A, Wege C, Gosele U, Jeske H, Nielsch K. Atomic layer deposition on biological macromolecules: metal oxide coating of tobacco mosaic virus and ferritin. Nano Lett 2006;6:1172–7.
[20] Yamashita I, Hayashi J, Hara M. Bio-template synthesis of uniform CdSe nanoparticles using cage-shaped protein, apoferritin. Chem Lett 2004;33:1158–9.
[21] Hrapovic S, Liu YL, Male KB, Luong JHT. Electrochemical biosensing platforms using platinum nanoparticles and carbon nanotubes. Anal Chem 2004;76:1083–8.
[22] Gider S, Awschalom DD, Douglas T, Mann S, Chaparala M. Classical and quantum magnetic phenomena in natural and artificial ferritin proteins. Science 1995;268:77–80.
[23] Meldrum FC, Heywood BR, Mann S. Magnetoferritin: in vitro synthesis of a novel magnetic protein. Science 1992;257:522–3.
[24] Liu G, Wu H, Wang J, Lin Y. Apoferritin-templated synthesis of metal phosphate nanoparticle labels for electrochemical immunoassay. Small 2006;2:1139–43.
[25] Aime S, Frullano L, Crich SG. Compartmentalization of a gadolinium complex in the apoferritin cavity: a route to obtain high relaxivity contrast agents for magnetic resonance imaging. Angew Chem Int Ed 2002;41:1017–9.
[26] Zhang LB, Laug L, Munchgesang W, Pippel E, Gosele U, Brandsch M, et al. Reducing stress on cells with apoferritin-encapsulated platinum nanoparticles. Nano Lett 2010;10:219–23.
[27] Watanabe A, Kajita M, Kim J, Kanayama A, Takahashi K, Mashino T, et al. In vitro free radical scavenging activity of platinum nanoparticles. Nanotechnology 2009;20:455105.
[28] Kajita M, Hikosaka K, Iitsuka M, Kanayama A, Toshima N, Miyamoto Y. Platinum nanoparticle is a useful scavenger of superoxide anion and hydrogen peroxide. Free Radic Res 2007;41:615–26.
[29] Roberts RA, Laskin DL, Smith CV, Robertson FM, Allen EMG, Doorn JA, et al. Nitrative and oxidative stress in toxicology and disease. Toxicol Sci 2009;112:4–16.
[30] Mates JM. Effects of antioxidant enzymes in the molecular control of reactive oxygen species toxicology. Toxicology 2000;153:83–104.
[31] Dickerson MB, Sandhage KH, Naik RR. Protein- and peptide-directed syntheses of inorganic materials. Chem Rev 2008;108:4935–78.
[32] Michaelis L, Menten ML. Die kinetik der invertinwirkung. Biochem Z 1913;49:333–69.
[33] Sen F, Gokagac G. Different sized platinum nanoparticles supported on carbon: an XPS study on these methanol oxidation catalysts. J Phys Chem C 2007;111:5715–20.
[34] Kim KS, Winograd N, Davis RE. Electron spectroscopy of platinum–oxygen surfaces and application to electrochemical studies. J Am Chem Soc 1971;93:6296–7.
[35] Borthiry GR, Antholine WE, Kalyanaraman B, Myers JM, Myers CR. Reduction of hexavalent chromium by human cytochrome b5: generation of hydroxyl radical and superoxide. Free Radic Biol Med 2007;42:738–55.
[36] Hu CC, Liu KY. Voltammetric investigation of platinum oxides. I. effects of ageing on their formation/reduction behavior as well as catalytic activities for methanol oxidation. Electrochim Acta 1999;44:2727–38.
[37] Switala J, Loewen PC. Diversity of properties among catalases. Arch Biochem Biophys 2002;401:145–54.
[38] Metelitsa DI, Arapova GS. Ferritin–a biocatalyst of aromatic amine oxidation. Biokhimiia 1996;61:308–21.